# Variable freshwater influences on the abundance of *Vibrio vulnificus* in a tropical urban estuary

Olivia D. Nigro[1], La'Toya I. James-Davis[2,3†], Eric Heinen De Carlo[3], Yuan-Hui Li[3], Grieg F. Steward[2,3*]

[1]Department of Natural Science, Hawai'i Pacific University, Honolulu, HI

[2]Daniel K. Inouye Center for Microbial Oceanography—Research and Education, School of Ocean and Earth Science and Technology (SOEST), University of Hawai'i at Mānoa, Honolulu, Hawai'i

[3]Department of Oceanography, School of Ocean and Earth Science and Technology (SOEST), University of Hawai'i at Mānoa, Honolulu, Hawai'i

[†]Present address: 3551 Roger Brooke Drive, JBSA Ft. Sam Houston, San Antonio, TX 78234

* Contact: Phone 808-354-1652; email grieg@hawaii.edu

## ABSTRACT

To better understand the controls on the opportunistic human pathogen *Vibrio vulnificus* in warm tropical waters, we conducted a year-long investigation in the Ala Wai Canal, a channelized estuary in Honolulu, HI. The abundance of *V. vulnificus* as determined by qPCR of the hemolysin gene (*vvhA*), varied spatially and temporally nearly four orders of magnitude (≤ 3 to 14,000 $mL^{-1}$). Unlike in temperate and subtropical systems, temperatures were persistently warm (19–31°C) and explained little of the variability in *V. vulnificus* abundance. Salinity (1–36 ppt) had a significant, but non-linear, relationship with *V. vulnificus* abundance with highest *vvhA* concentrations (> 2,500 $mL^{-1}$) observed only at salinities from 7 to 22 ppt. *V. vulnificus* abundances were lower on average in the summer dry season when waters were warmer but more saline. Highest canal-wide average abundances were observed during a time of modest rainfall when moderate salinities and elevated concentrations of reduced nitrogen species and silica suggested a groundwater influence. Distinguishing the abundances of two genotypes of *V. vulnificus* (C-type and E-type) suggest that C-type strains, which are responsible for most human infections, were usually less abundant (25% on average), but their relative contribution was greater at higher salinities, suggesting a broader salinity tolerance. Generalized regression models suggested up to 67% of sample-to-sample variation in log-transformed *V. vulnificus* abundance was explained (n = 202) using the measured environmental variables, and up to 97% of the monthly variation in canal-wide average concentrations (n = 13) was explained with the best subset of four variables.


## IMPORTANCE

Our data illustrate that, in the absence of strong seasonal variation in water temperature in the tropics, variation in salinity driven by rainfall becomes a primary controlling variable on *V. vulnificus* abundance. There is thus a tendency for a rainfall-driven seasonal cycle in *V. vulnificus* abundance that is inverted from the

48 temperature-driven seasonal cycle at higher latitudes. However, stochasticity in
49 rainfall and its non-linear, indirect effects on *V. vulnificus* concentration means that
50 high abundances can occur at any location in the canal at any time of year, making it
51 challenging to predict concentrations of this pathogen at high temporal or spatial
52 resolution. Much of the variability in canal-wide average concentrations, on the
53 other hand, was explained by a few variables that reflect the magnitude of
54 freshwater input to the system, suggesting that relative risk of exposure to this
55 pathogen could be predicted for the system as a whole.

56 **INTRODUCTION**

57 The bacterium *V. vulnificus* is an opportunistic and formidable human
58 pathogen that has a world-wide distribution, in a variety of marine and estuarine
59 environments (1). In humans, *V. vulnificus* may cause a range of illnesses that
60 includes gastroenteritis, necrotizing fasciitis, and septicemia (2). Infections occur as
61 a result of ingestion of contaminated seafood (3) or via wound exposure to waters
62 (4). Strains vary in their propensity to cause disease in humans, with certain
63 genotypically distinguishable strains much more commonly, but not exclusively,
64 associated with disease in humans (5). The exact mechanisms of virulence in *V.*
65 *vulnificus*, and the genes responsible for the onset of illness, have yet to be
66 determined, but a number of correlative biomarkers have been used to discriminate
67 those strains most commonly associated with human disease (6). Variations in the
68 16S rRNA gene, for example, have been used in PCR assays to discriminate "A-type"
69 strains from "B-type" strains (7, 8), the latter of which predominate among clinical
70 isolates. Another commonly used marker is the 200 bp segment of the virulence-
71 correlated gene that resolves the gene variants *vcgC* or "C-type" strains from *vcgE* or
72 "E-type" strains (9). PCR-based analysis of fifty-five *V. vulnificus* isolates indicated
73 that 90% of the strains isolated from infected patients were of the C-type (clinical),
74 while 93% of the strains isolated from the environmental samples were E-type
75 (environmental). Subsequent analyses revealed broader genomic differences along
76 with physiological differences between these lineages suggesting that they are

distinct ecotypes that may be better adapted for either environmental growth (E-type) vs. stress tolerance (C-type) (10). These biomarkers are largely congruent, with the common environmental strains being A-type/E-type, and the majority of clinical isolates being B-type/C-type, although all types can cause disease in humans (11).

Studies of *V. vulnificus* in temperate and subtropical waters have shown that warmer temperatures increase the frequency of detection (12–15). Quantification over an annual cycle reveals a clear temperature-driven seasonal signal, with the highest concentrations of *V. vulnificus* occurring in warm summer months (16–19) and culturable cells declining dramatically at temperatures below 13 °C (6). *V. vulnificus* abundance is also influenced by salinity (19–21), thriving in conditions of both warm temperatures and moderate salinities (5). The environmental patterns of abundance are consistent with observations of *V. vulnificus* growth under controlled laboratory conditions (12, 22) that show increasing growth rates up to around 37 °C, and a broad salinity tolerance with fastest growth rates between 5–25 ppt. Correlation models of environmental data support the idea that temperature and salinity are two of the most important variables controlling *V. vulnificus* abundance, but their relative importance depends on the ranges over which they are sampled . (21, 23–26).

In temperate environments, the incidence of *V. vulnificus* infection tracks the seasonal environmental abundances of the pathogen, with the most infections occurring during the warm summer months (6). It follows that the inhabitants of sub-tropical, and especially tropical areas, where air and water temperatures are warm year-round, would be particularly vulnerable to *V. vulnificus* infection. Indeed, according to available surveillance data for the years 2003–2008 (27–29), Hawai‘i had the fifth highest incidence of non-food-borne *V. vulnificus* infections in the U.S., trailing only four gulf states (Florida, Louisiana, Mississippi, and Texas). When we convert these to a per capita basis, it was the highest in the nation. Despite higher incidence of *V. vulnificus* wound infections, primarily from recreational waters, there has been little data collected on *Vibrio vulnificus* in the coastal waters of Hawai‘i (30, 31) and scant data on the ecology of *V. vulnificus* in tropical waters in general (20).

Consequently, we initiated an investigation of the abundance and dynamics of *V. vulnificus* in the Ala Wai Canal and Harbor.

The Ala Wai canal provides partially channelized drainage for two watersheds. Although it is not designated as a recreational waterway, the canal is used extensively for boating and fishing. Flow down the canal varies as a function of tide and of rainfall, the latter driving surface runoff (streams and storm drains) and, with some hysteresis, groundwater seepage. Salinity varies widely in the canal, as a function of depth, overall stream flow, position in the canal relative to the freshwater sources, and tidal forcing. Water temperature, on the other hand, varies over a relatively narrow range compared to temperate systems. Because of the seasonality in rainfall in Hawaii, with higher precipitation in winter months (32), we hypothesized that there could be an inverse seasonal pattern in *V. vulnificus* abundance driven by salinity compared to the strongly temperature-driven patterns in temperate waters.

Our objectives with this study were to document the temporal spatial variability of *V. vulnificus* total abundance and strain composition (C-type vs. E-Type) in the estuarine waters of the Ala Wai Canal and Harbor and to determine how abundance was related to environmental variables. The goal was to better understand the environmental controls on *V. vulnificus* in tropical estuarine waters and to assess the prospects for modeling pathogen abundance.

# MATERIALS AND METHODS

## Study Site

Sampling took place in the Ala Wai Canal (Fig. 1), a 3.1 km long, engineered waterway located on the southern coast of Oʻahu that separates Waikīkī and urban Honolulu (33). A watershed that covers 42.4 km$^2$ drains into the Ala Wai Canal via the Mānoa and Pālolo Streams, which merge to form the Mānoa-Pālolo Stream prior to entering the canal, and the Makiki Stream, all of which run through urban areas before reaching the canal. As a consequence, the streams are contaminated with a

variety of anthropogenic substances and their convergence in the Ala Wai Canal has contributed to its pollution and eutrophication (34, 35). The influx of fresh water from the streams creates a salinity gradient with a typical salt-wedge structure. Tidal flow causes seawater to flow landward on the flood tide and seaward on the ebb tide and remain at depth. The freshwater streams flow seaward on all tides creating a freshened water surface layer estimated to extend to 0.5 m depth on average, but which is highly variable both in salinity and thickness (36). Sediments are continually deposited in the canal at the mouth of the Mānoa-Pālolo Stream causing the build-up of a sill that restricts flushing of deep water in the uppermost section of the canal.

## Sampling locations, dates, and times

Sampling of the Ala Wai Canal spanned 13 months beginning March 17, 2008 and concluding on March 10, 2009, covering the nominal dry summer (April–September) and rainy winter (October–March) months. Samples were collected monthly at twelve sites in the Ala Wai Canal numbered (1 and 5–15) by distance from the shallow, upper section of the canal (Site 1) to the Ala Wai Harbor (Site 15). Site 9 was just inside the mouth of Mānoa-Pālolo Stream and Site 12 was at the mouth of Makiki Stream (Fig. 1, Supplemental Table S1). Missing site numbers 2–4 referred to other samplings at Site 1 that were not used in this study. Sampling at a higher temporal resolution was also conducted in the dry and rainy seasons to assess changes on shorter time scales. Samples were collected weekly at all sites for four weeks from June 26–July 17, 2008 and again for three weeks from February 22–March 10, 2009. Samples were also collected at a reduced number of sites (Sites 5, 9, 12, 14) daily for six days from July 10–15, 2008 and daily for five days from March 2–6, 2009, and once every three hours (trihoral) for twenty-four hours at Sites 5, 9, and 14 from July 15 to July 16, 2008.

## Rainfall and streamflow

Rainfall data collected by National Weather Service rain gauges (part of the Hawai‘i Hydronet System) at 15-minute intervals were retrieved from the online

resource (https://www.weather.gov/hfo/hydronet-data). Data from two gauges were selected for analysis. The first was HI-18 (NOAA# MNLH1), which is located near the origin of Mānoa Stream (N21.3161 W157.8142) at an elevation of 150 m in Manoa Valley ("Valley" rainfall). The second is HI-26 (ALOH1), which is located at Aloha Tower (N21.3060 W157.8662) in downtown Honolulu near sea level (15 m) at the coast ("Coastal" rainfall). From these data, average daily rainfall for all sampling months was determined, as well as total rainfall from each 24-hour period prior to sampling. Data on tidal flux were obtained from the National Ocean Service (NOS), using tide gauge number 1612340. Stream flow data were obtained from the United States Geological survey (waterdata.usgs.gov/usa/nwis/uv?16247100) for the Mānoa-Pālolo Stream gauge #16247100.

## Water sample collection and processing

Whole water samples were collected from the top 10–30 cm at all sites in acid-washed bottles with a pole sampler and stored on ice (except for samples used for culturing, which were kept at ~15 °C with cold packs) and transported to the laboratory within three hours of collection. Subsamples (ca. 25 mL) for nutrient analysis (n = 207–211) were frozen and shipped on dry ice to the Oregon State University nutrient analysis facility for determination of dissolved silica, phosphate, nitrate plus nitrite, nitrite, and ammonium concentrations (37). Nutrient concentrations were measured during every sampling event excluding two weekly sampling events in July 2008 (July 3 and 7). The values for the mean, number of samples, median, minimum and maximum of the measured nutrients have been previously reported (38).

For particulate carbon (PC) or nitrogen (PN) and chlorophyll a (chl a) measurements, subsamples (25–200 ml) were filtered onto pre-combusted glass-fiber filters (GF/F, Whatman) in duplicate and stored frozen until analysis. For PC and PN (n = 199), filters were pelletized and combusted in a high-temperature combustion CN analyzer, the CE-440 CHN elemental analyzer (Exeter Analytical) following HOT program protocols (39). Filters for chl a analysis (n = 194) were extracted in 100% acetone at -20°C for 7 days. Fluorescence of extracts and

195 standards were measured using a Turner AU10 fluorometer before and after
196 acidification (40).
197 Samples for bacteria counts (n = 219) were fixed with filtered (0.2 µm)
198 formaldehyde (10% w/v final concentration) in a cryovial (Nalgene) and stored at -
199 80 °C. Total bacteria were counted by thawing samples, staining with SYBR Green I,
200 and analyzing on an acoustic focusing flow cytometer (Attune; Thermo Fisher
201 Scientific).
202 Samples for molecular analysis (100– 550 mL) were pressure filtered via
203 peristaltic pump through 0.22 µm polyethersulfone filter capsule (Sterivex,
204 Millipore), then stored at -80 °C until extracted.

205 **Cultivation on vibrio selective medium**

206 For five of the monthly samplings (Mar, Jun, Sep, Dec 2008, and Mar 2009),
207 water samples were filtered through 0.45 µm pore size, mixed cellulose ester filters
208 (47 mm, GN-6; Pall) and filters were placed face-up on the vibrio-selective medium
209 CHROMagar Vibrio (DRG Intl.). After overnight incubation, blue colonies were
210 enumerated as putative *V. vulnificus*.

211 **DNA extraction and purification**

212 DNA was extracted from the Sterivex filters using the Masterpure™ Nucleic
213 Acid Extraction Kit (Epicentre). Six-hundred microliters of Masterpure™ Tissue and
214 Cell Lysis Solution containing recommended quantities of proteinase K were added
215 to each Sterivex filter. The ends of the filters were sealed and the filters incubated
216 on a rotisserie in a hybridization oven at 65 °C for 15 minutes. Fluid was recovered
217 from filter housing by aspiration with a syringe. The filling with buffer, incubation,
218 and buffer recovery steps were repeated twice more and the combined extract from
219 all three rounds was pooled (total volume ca. 1.8 ml). Three-hundred microliters of
220 the pooled extract was processed according to the Masterpure™ Kit guidelines and
221 the remainder was archived. Accounting for all of the raw extract volume, total DNA
222 yields ranged from 1–540 µg $L^{-1}$ of canal water (geometric mean of 30 µg $L^{-1}$).
223 Following initial purification, the resuspended DNA (200 µL) was passed through a

spin column containing acid-washed polyvinylpolypyrrolidone (PVPP) in an effort to remove any residual inhibitors (41). DNA concentration in each sample was quantified fluorometrically (Quant-iT Broad Range DNA kit, Life Technologies) both before and after the PVPP purification step to account for losses incurred during the purification stage (average recovery 60%). Geometric mean concentration of DNA in the final purified extracts was 7 ng $\mu L^{-1}$ (range 0.1–54 ng $\mu L^{-1}$).

## Quantitative PCR

Total *V. vulnificus* was estimated by TaqMan qPCR targeting the hemolysin gene (*vvhA*) using primer and probe sequences reported by Campbell and Wright (42). Quantification of C-type *V. vulnificus* used the primers and probes targeting the virulence-correlated gene variant (*vcgC*) from Baker-Austin et al. (43). E-type *V. vulnificus* was calculated as the difference in concentration between the two assays. Both assays were prepared as 25-µL reactions with 12.5 µL of TaqMan Universal PCR Master Mix (Applied Biosystems), 1.5 µg $\mu l^{-1}$ final concentration of non-acetylated bovine serum albumin (Applied Biosystems) and 0.25–0.9 µM each of the appropriate primers and probe (Supplemental Table S2), 2–5 µl of DNA template, and water as needed. For *vvhA* assay, primers were added at 0.9 µM each and the probe at 0.25 µM. For the *vcgC* assay, primers and probe were each added at 0.5 µM final concentrations. Cycling conditions consisted of initial denaturation at 95 °C (10 min), then 40 cycles of 95 °C (15 s) and 60 °C (60 s). All qPCR reactions were performed in triplicate with DNA template in the final replicate diluted 10-fold (up to 50-fold) to check for inhibition (44) and with additional replication as needed to repeat inhibited samples at the higher dilutions. The cycling protocol consisted of an initial denaturation at 95 °C for 10 minutes, followed by 40 cycles of 95 °C for 15 s and 60 °C for 60–90 s. The amplified PCR product was detected by monitoring the increase in fluorescence signal generated from the 6-carboxyfluorescein-labeled probe using a Realplex$^2$ Mastercycler (Eppendorf). Data were analyzed using realplex software (Eppendorf) to determine cycle threshold ($C_t$) values. A standard curve of serial 10-fold dilutions of genomic DNA (*V. vulnificus* strain YJ016) was run in triplicate along with the samples.

## Statistical treatment of data

Statistical analyses were conducted using JMP Pro 15 (SAS Institute, Inc.). Concentrations of *V. vulnificus* (CFU or *vvhA* gene copies $mL^{-1}$), total bacteria, chl *a*, nutrients, PC, and PN were log transformed and rainfall and streamflow were cube-root transformed in order to normalize the data for multivariate analyses. For some analyses, sites were clustered into categories of "Upper canal" (Sites 1, 5–8) and "Lower canal" (Sites 10, 11, 13–15) based on whether they were landward or seaward of the sediment sill deposited at the mouth of the Mānoa-Pālolo Stream. Comparison of means between two samples were conducted with t-tests assuming unequal variance or by the non-parametric Komlgorov-Smirnov Asymptotic Test for data that could not be readily normalized by transformation. Comparisons of means among three or more samples were conducted by ANOVA with a post-hoc Tukey-Kramer test of honestly significant difference. Factor analysis was conducted on *vvhA* and nutrient data using principal components with varimax rotation. For multiple linear regression, the data were split into two subsets (salinity < 12 or ≥12 ppt), because of the non-linearity in the relationship between *V. vulnificus* and salinity (21). Multiple linear regression models were also conducted on data covering the entire salinity range by either including a quadratic term for salinity (24, 45) or a derived variable $\mathbf{\Delta}Sal_{opt}$, which is the absolute value of difference between the sample salinity and an optimum salinity set as 12 ppt (46). Variables for constructing generalized regression models on each subset were selected using the Akaike Information Criterion by screening for the subsets that produced the best fit among all possible models. Among equivalent subsets in the "green zone" (AICc to AICc+4), either the subset with the best fit or with the fewest variables was selected as noted in the text.

Out of 243 total qPCR assays for *V. vulnificus* abundance, seventeen (ca. 7%) had issues that made them unreliable or unavailable (inhibition, below the reporting limit for the assay, or absence of data). In thirteen of these instances, abundances were instead inferred from blue colony counts on CHROMagar Vibrio medium (Supplemental Methods), based on the strong correlation (r = 0.8) between log-

transformed concentrations of blue colony counts and vvhA gene copy numbers (Supplemental Fig. S1).

# RESULTS

## Variability of the habitat

Rainfall in Mānoa Valley, one of the major watersheds draining into the canal, varied from 0 to 15.8 cm in the 24-hour period preceding each sampling event. The average rainfall prior to samplings in the rainy season (Oct–Mar) was 3.7 cm, which was significantly higher (p = 0.0054) by an order of magnitude compared to the average in the dry season (Apr–Sep) of 0.27 cm (Supplemental Figure S2). Flow from the Mānoa-Pālolo Stream varied from 0.4 to 2.6 $m^3 s^{-1}$ on sampling days and was strongly correlated with the prior 24-hr rainfall in Mānoa Valley (r = 0.87, n = 13, $p$ = <0.0001; Supplemental Table S3). Both the canal-wide average salinity and temperature for the monthly samplings (n = 13) had significant negative correlations with prior 24-hr rainfall (r = -0.84, $p$ = 0.0003 and r = -0.86, $p$ = 0.0002, respectively).

Over the course of the 13-month study, measured surface water salinities in the Ala Wai Canal varied from 1 to 36 ppt (mean of 24 ppt) and temperatures from 19.2 to 31.8 °C (mean of 27 °C; Table 1). Salinity was highly variable throughout the study area reaching maxima of ≥ 29 ppt at every site and minima of ≤ 5 ppt at least once at each site except Site 15, which is the most seaward site in the harbor (minimum salinity of 11 ppt). Consequently, there was no significant difference in average salinity among sites (ANOVA, $p$ > 0.07). When samples were clustered by general location, average salinity in the upper and lower canal were not significantly different ($p$ = .7818), but the combined stream mouth sites had significantly lower salinity on average than either the upper (p = .0083) or lower (p = .0016) canal sites.

All of the measured variables (Table 1) except silica and nitrite displayed overall significant positive or negative significant correlations with salinity (Supplemental Table S4), but the correlation coefficients were low in many cases

because of non-linearity in the relationships (Fig. 2). Temperature displayed a significant, linear positive correlation with salinity ($r = 0.65$, $n = 242$, $p < .0001$). Correlation and regression analyses for all other variables vs. salinity are reported for log transformed data. Concentrations of chl *a* (range 0.4–512 μg $L^{-1}$) showed a significant positive, linear (Fig. 2a) correlation with salinity ($r = 0.49$, $n = 194$, $p < 0.0001$). Concentrations of total bacteria (range $0.47 \times 10^6$ to $11 \times 10^6$ $mL^{-1}$) also showed a significant positive correlation with salinity ($r = 0.29$, $n = 219$; $p < 0.0001$), but the relationship was non-linear (Fig. 2c). Particulate carbon (range 15–5,600 μM) had a non-linear relationship with salinity (Fig. 2d) that resulted in an overall weak but significant negative correlation ($r = -0.25$, $n = 199$, $p = 0.0003$).

Of the dissolved inorganic nutrients, only phosphate (range 0.2–8.7 μM) had a linear relationship with salinity (Fig. 2e) and displayed a significant negative correlation ($r = -0.46$, $n = 211$, $p < 0.0001$). Concentrations of silica (11–490 μM), nitrate (0.02–260 μM), nitrite (0.04–3.3 μM), and ammonia (0.94–22 μM) all displayed significant, non-linear relationships with salinity (Fig. 2f-i), with highest values occurring at moderate salinities. Despite the non-linear relationships, there were significant negative correlations between salinity and either nitrate ($r = -0.32$, $p < 0.0001$) or ammonia ($r = -0.44$, $p < 0.0001$). Silica and nitrite, on the other hand, showed highly significant, non-linear relationships with salinity (Fig. 2f, h), that resulted in low and insignificant correlation coefficients.

When sites were clustered by location, most nutrients (nitrate, ammonia, phosphate, silica, but not nitrite), particulate carbon, chl *a*, and total bacteria were all significantly higher ($p < 0.01$) in the upper canal sites than the lower canal sites.

## Temporal and spatial variability of *V. vulnificus*

Concentrations of the *vvhA* gene (a proxy for *V. vulnificus* abundance) varied over several orders of magnitude in space and over time (Fig. 3) from 3 to 13,700 $mL^{-1}$ with overall geometric mean concentration for all samplings of 68 $mL^{-1}$ ($n = 239$; Table 1). Concentrations of *vvhA* at any given site were highly variable over time with values that were above average or below average occurring at some point at every location. Although spatial and temporal variability were low during the

342 trihoral sampling over the course of one day in July, larger variations were seen on
343 daily or longer time scales. The most dramatic variation is the change from above
344 average to below average concentrations at every site in the span of 15 days
345 (October 27 to November 11, 2008).

346 Despite the high variability, average log-transformed *vvhA* concentrations in
347 the rainy season (1.98 ± 0.72) were significantly higher (unpaired t-test, $p = .0013$)
348 than the dry season (1.72 ± 0.50; Supplemental Fig. S2). None of the individual
349 sites had an annual average *vvhA* concentration that was significantly different from
350 any of the others (ANOVA, post-hoc Tukey, $p \geq .63$). However, excluding the stream
351 mouth sites, the annual average concentration of log-transformed *vvhA* for the five
352 sites in the upper canal (2.04 ± 0.74) was significantly higher (n = 65 at each site;
353 unpaired t-test, $p = .0110$) than the annual average for five sites in the lower canal
354 (1.75 ±0.70).

355 **Relationship of *V. vulnificus* to temperature and salinity**

356 Log-transformed concentrations of *vvhA* displayed a weak, but significant,
357 negative correlation (r = -0.174, $p = .0071$) with temperature (Fig 4a). However,
358 partial correlation analysis indicates that the relationship between log[*vvhA*] and
359 temperature is weakly positive, but significant (r = 0.258, $p < .0001$) when
360 accounting for the effect of salinity and other variables. The relationship of
361 log[*vvhA*] with salinity was non-linear with a peak around 12 ppt (Fig. 4b). Linear
362 regression analysis for samples having a salinity either < 12 or ≥ 12 ppt showed that
363 *vvhA* increased significantly ($r^2 = 0.315$; F test, $p = .0001$) as a function of salinity
364 over the lower range and decreased significantly ($r^2 = 0.492$; F test $p < .0001$) over
365 the higher range.

366 Concentrations of clinical, or C-type, *V. vulnificus* were usually lower than
367 those of environmental, or E-type, and accounted for 26% of the total *V. vulnificus* on
368 average across all samplings for which data were available (n = 219), indicating that
369 communities were most often dominated by E-type. Both C-type and E-type *V.*
370 *vulnificus* were most abundant at moderate salinities and declined as a function of

371 salinity, but C-type declined at a lower rate. As a result, the contribution of C-type
372 tended to increase as a function of salinity. Samples in which C-type accounted for
373 >50% of the total (n = 39) were only observed in higher salinity waters (Fig. 4b) and
374 the % C-type was significantly higher (Komolgorov-Smirnov; $p = 0.0164$) in higher
375 salinity samples (≥ 25 ppt, n = 146) than in samples having lower salinity (< 25 ppt,
376 n = 73; Supplemental Fig. S3).

377 **Relationship between *V. vulnificus* and additional variables**

378 To understand additional factors that may be important in controlling *V.*
379 *vulnificus* in this habitat, factor analysis was conducted with *vvhA*, temperature,
380 salinity, and nutrient data (Fig. 5a). Two factors had eigenvalues > 1. The strongest
381 positive correlations (r ≥ 0.4) were between *vvhA* and silica or reduced nitrogen
382 species, which were associated with Factor 1, and strong negative correlations (r ≤ -
383 0.4) were found between salinity and *vvhA*, ammonia, and phosphate along Factor 2.
384 Plots of the factor loading values with points coded by rainfall and streamflow (Fig
385 5b) illustrate the relationship between indicators of freshwater input and salinity
386 along the Factor 2 axis. Coding the points by log *vvhA* concentration and silica
387 concentration illustrates the association of these variables (along with reduced
388 nitrogen species) with Factor 1. Overall the highest concentrations of *vvhA* occurred
389 at moderate rainfall in the valley, but relatively low streamflow, and elevated
390 concentrations of silica.

391 Generalized regression models for predicting *vvhA* concentrations over the
392 two different salinity ranges were constructed using the overall best subset (<12
393 ppt model) or the best subset having the minimum number of variables (≥ 12 ppt
394 model). Only properties intrinsic to the individual samples were included in this
395 analysis (i.e., tides, rainfall and streamflow were not considered). For samples with
396 salinities < 12 ppt (n = 39 out of 41 samples, because of missing nutrient data) a
397 subset of four (temperature, nitrite, silica, and PC) out of eight variables explained
398 75% of the observed variation with the equation:
399
400 $$log[vvhA] = 0.154 \bullet T + 1.015 \bullet log[nitrite] - 0.600 \bullet log[silica] - 0.850 \bullet log[PC] + 2.170$$

where $T$ is temperature in °C, and nitrite, silica, and particulate carbon (PC) are in units of µM (model fit illustrated in Supplemental Fig S4a). For samples with salinities ≥ 12 (n = 163 out of 198 possible samples because of missing nutrient data) a subset of just three (temperature, salinity and phosphate) out of seven variables explained 55% of the variability:

$$log[vvhA] = 0.0360 \bullet T - 0.0727 \bullet S + 0.515 \bullet log[phosphate] + 2.835$$

where $T$ is temperature in °C, $S$ is salinity is in units of ppt, and phosphate is in units of µM (model fit illustrated in Supplemental Fig. S4b). PC was removed prior to variable selection in the latter model, because initial analysis showed it offered no significant explanatory power at salinities >12 ppt, and missing data would have further restricted the samples included in the analysis. When predictions from the two models were combined, 66% of the variability in log(*vvhA*) over the entire salinity range was explained overall (Fig. 6).

Models in which either a quadratic term for salinity or the derived variable $\Delta Sal_{opt}$ were included explained similar amounts of variability ($r^2$ = 0.61 and 0.63, respectively; $p \leq .0001$) using different sets of five variables (Supplemental Fig. S5), but were slightly outperformed by the combined models above.

## System-wide controls on *V. vulnificus*

To smooth out inter-station variability and focus on temporal variations in *vvhA*, canal-wide averages for the variables for each monthly sampling were also analyzed in relation to system-wide drivers of rainfall and streamflow (Fig. 7). In general, average rainfall, streamflow, phosphate, silica, and *vvhA* are all below average, and salinity above average, during most of the dry season with minimal variability. During the rainy season, periodic heavy rainfall resulted in high variability with excursions in all variables well above and below their overall averages.

Three freshening events are evident from dips in the average salinity in the canal during the rainy season (Fig. 7). The first begins in September and peaks in October 2008 following increases in rainfall and streamflow. The average monthly rainfall increased from ≤ 0.75 cm $d^{-1}$ in the preceding months to 1.0 cm $d^{-1}$ in Sep–Oct, and the 24-hour antecedent rainfall for the October sampling was 2 cm (up from ≤ 0.5 cm in other samplings). Streamflow increased from 0.4 $cm^3$ $s^{-1}$ in July–August to 0.7–0.8 $cm^3$ $s^{-1}$ in Sep–Oct. Despite these relatively modest increases, canal-wide average salinity dropped to 8 ppt and the average silica concentrations in Sep–Oct reached their highest concentrations (223–244 µM). Phosphate displayed only a small local peak in average concentration (2 µM). Canal-wide average concentrations of *vvhA* reached a maximum during this event from 350 (range 67–3,500 gene copies $mL^{-1}$ in September to an average of 2,700 (range 170 to 13,700) gene copies $mL^{-1}$ in October. The average concentration in October was significantly higher than at any other monthly sampling (ANOVA, post-hoc Tukey, $p \leq .0005$). At the subsequent sampling 15 days later (November), rainfall had stopped, streamflow, phosphate and silica had declined, average salinity had increased to 29 ppt and *vvhA* was at the lowest average concentration of the study with an average of 20 (range 7–63) gene copies $mL^{-1}$ across all sites.

A second, more pronounced drop in salinity occurred in December 2008 in response to heavy rainfall recorded at both the coastal and Mānoa valley rain gauges, resulting in the highest recorded streamflow (2.6 $m^3$ $s^{-1}$), minima in salinity (3 ppt) and silica (34 µM), and the highest average phosphate concentration (2.9 µM). In contrast to the previous freshening event, *vvhA* was not significantly elevated (61 gene copies $mL^{-1}$) and was near the overall study average.

A third freshening event occurred at the time of the last sampling in March 2009 as a result of heavy rainfall in Mānoa Valley, but not at the coast. Streamflow (1.3 $m^3$ $s^{-1}$) was above average and intermediate between the first and second events, and salinity was again significantly reduced (4 ppt). The effects on phosphate (1.3 µM) and silica (87 µM) were modest, with phosphate being just above the long-term average and silica just below. The mean concentration of *vvhA*

reached its third highest level at this time reaching 175 (range 22–811) gene copies $mL^{-1}$ after steadily increasing each month from the lowest value in November.

Multiple linear regression was used to determine which subset of variables best predicted canal-wide average log(*vvhA*) concentrations. The model resulting from the best subset out of all combinations of twelve possible variables was:

$$Log[vvhA]_{avg} = -1.125 \bullet Streamflow - 0.07633 \bullet Salinity + 0.00502 \bullet Silica + 0.00151 \bullet PC + 3.522$$

where streamflow is in units of $m^3\ s^{-1}$, and salinity, silica, and particulate carbon (PC) are in units of µM. All variables are the geometric means for all sites in the canal for each monthly sampling (n= 13). Linear regression of the observed vs. predicted *vvhA* suggests that 97% of the canal-wide average variation in *vvhA* could be explained with the selected variables (Fig. 8a).

A second simpler model using a minimum of readily measurable variables (salinity and rainfall) was also constructed:

$$Log[vvhA]_{avg} = -0.162 \bullet rainfall - 0.0956 \bullet salinity + 4.348$$

where rainfall is average rainfall in cm for the prior 24 hours at the Mānoa Valley gauge, and salinity is canal-wide average salinity in ppt. This simpler model explained 83% of the variability in average log-transformed concentrations of *vvhA* (Fig. 8b).

# DISCUSSION

## Temporal and spatial variability of *V. vulnificus*

*V. vulnificus*, as inferred from *vvhA* gene, was consistently detected throughout the year in the Ala Wai Canal and Harbor system, but varied dramatically over space and time. Sampling on different temporal scales showed minimal variation in *V. vulnificus* within a day, but dramatic and stochastic variations on longer time scales and among sites. This suggests that factors with

488 regular intra-day variations (e.g. tides, or daily changes in temperature and primary
489 productivity driven by insolation) had relatively little influence on concentrations of
490 *V. vulnificus*. The largest absolute change in the canal-wide average *vvhA*
491 concentrations seen over the entire study occurred in a span of 2 weeks. The
492 observation that *V. vulnificus* concentrations were higher on average in the rainy vs.
493 dry season, yet the lowest average concentration recorded in the study also
494 occurred in the rainy season within weeks of the highest abundances, suggests that
495 freshwater input, which occurs stochastically, but with an underlying strong
496 seasonal component, is the most significant contributor to variability in *V. vulnificus*
497 abundance in this environment.

498 The results support an earlier hypothesis (21) that in tropical and some
499 subtropical climates, where the temperature range is narrow and persistently
500 warm, salinity is a stronger determinant than temperature of *V. vulnificus*
501 abundance. This is consistent with the seasonal variation in *V. vulnificus* in oysters in
502 India, which is not related to temperature, but by summer monsoonal rains
503 lowering salinity (47). In Hawai‘i, with its rainy season in winter months, there is
504 thus a tendency toward a seasonal cycle in *V. vulnificus* abundance that is inverted
505 from the pronounced temperature-driven cycle found at higher latitudes and the
506 monsoon-driven cycle in India.

507 **Variable sources and influence of freshwater inputs**

508 The two major sources of freshwater to the Ala Wai canal are surface runoff
509 (primarily point source from streams and storm drains) and groundwater seeps.
510 Compared to surface runoff, groundwater in Hawai‘i tends to be enriched in silica as
511 a result of prolonged water-rock interactions (48) and depleted in phosphate as a
512 result of interactions with lateritic soils containing high concentrations of iron and
513 aluminum oxyhydroxides (48, 49). These differences, along with information on
514 rainfall and streamflow, are helpful in identifying the primary source of the
515 freshwater entering the canal. In the factor analysis, Factor 1 may be interpreted as
516 a latent variable for groundwater (high loading for silica, but low for phosphate),
517 and Factor 2 as a latent variable for (negative) surface runoff (high, but opposing,

518 loading of salinity and phosphate). Plots of the loading scores reinforce the
519 observation that *V. vulnificus* tended to be highest at moderate salinities and suggest
520 that groundwater was a relatively more important source of freshwater input under
521 those conditions (low streamflow, but elevated silica). When rainfall was highest,
522 surface runoff contributed more to freshwater input (highest streamflows with high
523 phosphate, low silica) and was associated with lower concentrations of *vvhA*.
524 This variable relationship between *vvhA* and freshwater source was also
525 discernible in the temporal changes in variables when averaged across all canal
526 sites. Of the three major freshening events, the first, with relatively high silica and
527 low phosphate, suggests a significant contribution from groundwater. This is
528 consistent with the observation of significant drops in salinity despite only modest
529 increases in stream flow compared to the summer months. This presumed increase
530 in groundwater input appears to have been driven by a moderate increase in
531 monthly average rainfall in both September and October, coupled with a modest
532 increase in average rainfall during the 24 hours preceding sampling that was
533 greater at higher elevations in the watershed than locally.
534 The second freshening event, with a high concentration of phosphate but low
535 silica, appears to be dominated by surface runoff, resulted from a Kona storm on the
536 south shore of Oahu (38). A Kona storm is a rain event that deviates from the
537 normal northeasterly trade-wind driven patterns that govern Hawaii's weather and
538 occurs when southwestern Kona winds bring heavy rains to the southern shore of
539 Oahu. This storm resulted in unusually high rainfall, both higher in the watershed
540 and locally, in the 24 hours prior to sampling.
541 The third freshening event on March 10, 2009 appears to have a source
542 signature that is intermediate to the two prior events in terms of stream flow and
543 silica. This is consistent with an average rainfall in the preceding 24 hours in the
544 watershed that was high enough to increase downstream runoff and groundwater
545 discharge into the canal (as in the previous event), but with limited local
546 precipitation that, unlike the previous event, did not contribute appreciably to
547 surface runoff.

548 The concentrations of *vvhA* during these three events suggest that the
549 magnitude, if not the sources, of the freshwater input to the canal has a large
550 influence on *V. vulnificus* abundances. The mixing of freshwater with the seawater in
551 the canal is expected to have competing influences on *V. vulnificus*, because it
552 simultaneously alters temperature, salinity, and residence time. At sustained,
553 moderate levels of freshwater input (such as that from ground water intrusion
554 driven by moderate rainfall higher in the watershed), both the temperature drop
555 and decrease in residence time are relatively small, but the freshening is sufficient
556 to result in salinities that are optimal for *V. vulnificus*, thus explaining the unusually
557 high abundance of *V. vulnificus* in September and October 2008. During unusually
558 intense storms, especially with high rainfall lower in the watershed (December
559 2008), the very high levels of surface runoff appear to suppress abundances of *V.*
560 *vulnificus* in the canal. This is likely a result of the simultaneous reduction in growth
561 rate (caused by decreases in both temperature and salinity to below optimum) and
562 reduced residence time of water in the canal. Gonzalez (1971)(36), for example,
563 observed an inverse relationship between streamflow and residence time of runoff
564 waters in the Ala Wai Canal.
565 Although intense storms can temporarily suppress the canal-wide average
566 concentrations of *V. vulnificus* in the canal/harbor system, the actual changes are
567 site-specific. We observed, for example, that during the December 2008 storm, *V.*
568 *vulnificus* abundance, despite a lower canal-wide average, was higher than average
569 at Site 15, the most seaward site located in the Ala Wai Boat Harbor. In this location,
570 salinity was temporarily reduced to 13 (in the optimal range for *V. vulnificus*)
571 compared to the typical average salinity for this site of ≥ 30 (38). Salinity remained
572 below the average in the harbor for 16 hours following the cessation of rainfall. This
573 suggests that the sites posing the highest risk of infection by *V. vulnificus* will vary
574 depending on the rainfall patterns and can even include the harbor which usually
575 had some of lowest concentrations. This condition-dependent elevated risk in the
576 harbor is consistent with the unfortunate incident of infection and death of an
577 individual who had open wounds exposed to harbor water following a long period
578 of intense rainfall (50).

## Patterns of *V. vulnificus* strain abundance

C-type *V. vulnificus* are the strains most frequently associated with infections in humans (9), but are often less abundant than E-type in environmental samples (9, 51). This appeared to be the case in our study site with C-type *V. vulnificus* accounting for an estimated 25% on average. The percentage was highly variable, however, and our observation that the C-type *V. vulnificus* tended to make up a higher percentage of the total at higher salinities (despite declining in absolute abundance) is consistent with some previous observations. Williams et al. (2017), for example, observed a negative influence of salinity on the abundance of E-type and C-type strains, but the effect was greater for E-type (51). Lin and Schwartz (2003) observed that when temperature decreased and salinity increased, in situ abundance of 16S rRNA A-type strains (analogous to E-type) decreased while B-type (analogous to C-type) increased and temporarily became the dominant genotype (52). Other studies in high salinity (> 32 ppt) coastal waters have found that either a majority (7) or all (53) of the isolates obtained were of B-type (C-Type). These observations support the contention that these different genotypes reflect distinct ecotypes, with the C-type having greater stress tolerance (10).

Multiple linear regression analysis was used to model *V. vulnificus* abundance using a reduced number of variables. Although these variables explained a significant percentage of the variability in *V. vulnificus* abundance, a great deal of sample-to-sample variability remains unexplained, which is not uncommon (21, 26). Predicting system-wide average concentrations of *V. vulnificus*, on the other hand, was much more successful. A model with the best subset of four variables explained 97% of the variability, and much simpler model relying on only two readily obtainable measurements (rainfall and salinity), still accounted for much of the variability and might prove more useful in practice for predicting relative risk from *V. vulnificus* of exposure to waters of the canal and harbor.

The high level of predictability for system-wide average *V. vulnificus* is similar to that achieved using logistic regression to predict *vvhA* as a binary response variable either as presence vs. absence (46) or low vs. high abundance (54). Improvements

609 in the prediction of *V. vulnificus* at higher resolution may be realized by combining
610 biological population models for *V. vulnificus* with physical models of coastal
611 circulation (54). In the meantime, the results from this study provide a detailed
612 description of the ecology of *V. vulnificus* in tropical estuarine waters of Hawai‘i. The
613 results are a useful first step toward predicting and, ultimately taking steps to
614 mitigate, the incidence of *V. vulnificus* infections.

615 ## ACKNOWLEDGMENTS

616 We are grateful to G. Walker and B. Marchant for assistance with sample collection
617 and A. Culley for support and advice. We thank Hawai‘i Ocean Time-series program
618 staff for support with processing PC/PN samples and R. Briggs for advice on
619 chemical measurements. This work was supported by grants from Hawai‘i Sea Grant
620 (2009, 2012) and the National Science Foundation (OCE05-54768, OCE08-26650)
621 and NOAA Ocean Observing (NA07NOS4730207).

622 ## REFERENCES

623 1. Oliver J. 2006. *Vibrio vulnificus*, p. 349–363. *In* Thompson, F, Austin, B, Swings, J
624 (eds.), The Biology of Vibrios. American Society for Microbiology (ASM),
625 Washington, D.C.

626 2. Horseman MA, Surani S. 2011. A comprehensive review of *Vibrio vulnificus*: an
627 important cause of severe sepsis and skin and soft-tissue infection. Int J Infect
628 Dis 15:e157–e166.

629 3. Jones MK, Oliver JD. 2009. *Vibrio vulnificus*: disease and pathogenesis. Infect
630 Immun 77:1723–1733.

631 4. Oliver JD. 2005. Wound infections caused by *Vibrio vulnificus* and other marine
632 bacteria. Epidemiol Infect 133:383–391.

633 5. Oliver JD. 2015. The biology of *Vibrio vulnificus*. Microbiol Spectr 3:VE-0001-
634 2014.

635 6. Baker-Austin C, Oliver JD. 2018. *Vibrio vulnificus*: new insights into a deadly
636 opportunistic pathogen. Environ Microbiol 20:423–430.

637 7. Kim MS, Jeong HD. 2001. Development of 16S rRNA targeted PCR methods for
638 the detection and differentiation of *Vibrio vulnificus* in marine environments.
639 Aquaculture 193:199–211.

640 8. Nilsson WB, Paranjype RN, DePaola A, Strom MS. 2003. Sequence
641 polymorphism of the 16S rRNA gene of *Vibrio vulnificus* is a possible indicator
642 of strain virulence. J Clin Microbiol 41:442–446.

643 9. Rosche TM, Yano Y, Oliver JD. 2005. A rapid and simple PCR analysis indicates
644 there are two subgroups of *Vibrio vulnificus* which correlate with clinical or
645 environmental isolation. Microbiol Immunol 49:381–389.

646 10. Rosche TM, Binder EA, Oliver JD. 2010. *Vibrio vulnificus* genome suggests two
647 distinct ecotypes. Environ Microbiol Rep 2:128–132.

648 11. Sanjuán E, Fouz B, Oliver JD, Amaro C. 2009. Evaluation of genotypic and
649 phenotypic methods to distinguish clinical from environmental *Vibrio vulnificus*
650 strains. Appl Environ Microbiol 75:1604–1613.

651 12. Kelly MT. 1982. Effect of temperature and salinity on *Vibrio* (*Beneckea*)
652 *vulnificus* occurrence in a Gulf Coast environment. Appl Environ Microbiol
653 44:820–824.

654 13. O'Neill KR, Jones SH, Grimes DJ. 1992. Seasonal incidence of *Vibrio vulnificus* in
655 the Great Bay estuary of New Hampshire and Maine. Appl Environ Microbiol
656 58:3257–3262.

14. Kaysner CA, Abeyta C, Wekell MM, DePaola A, Stott RF, Leitch JM. 1987. Virulent strains of *Vibrio vulnificus* isolated from estuaries of the United States West Coast. Appl Environ Microbiol 53:1349–1351.

15. Høi L, Larsen JL, Dalsgaard I, Dalsgaard A. 1998. Occurrence of *Vibrio vulnificus* biotypes in Danish marine environments. Appl Environ Microbiol 64:7–13.

16. Motes ML, DePaola A, Cook DW, Veazey JE, Hunsucker JC, Garthright WE, Blodgett RJ, Chirtel SJ. 1998. Influence of water temperature and salinity on *Vibrio vulnificus* in Northern Gulf and Atlantic Coast oysters (*Crassostrea virginica*). Appl Environ Microbiol 64:1459–1465.

17. Lin M, Payne DA, Schwarz JR. 2003. Intraspecific diversity of *Vibrio vulnificus* in Galveston Bay water and oysters as determined by randomly amplified polymorphic DNA PCR. Appl Environ Microbiol 69:3170–3175.

18. Pfeffer CS, Hite MF, Oliver JD. 2003. Ecology of *Vibrio vulnificus* in estuarine waters of eastern North Carolina. Appl Environ Microbiol 69:3526–3531.

19. Randa MA, Polz MF, Lim E. 2004. Effects of temperature and salinity on *Vibrio vulnificus* population dynamics as assessed by quantitative PCR. Appl Environ Microbiol 70:5469–5476.

20. Rivera S, Lugo T, Hazen TC. 1989. Autecology of *Vibrio vulnificus* and *Vibrio parahaemolyticus* in tropical waters. Water Res 23:923–931.

21. Lipp E, Rodriguez-Palacios C, Rose J. 2001. Occurrence and distribution of the human pathogen *Vibrio vulnificus* in a subtropical Gulf of Mexico estuary. Hydrobiologia 460:165–173.

22. Chase E, Harwood VJ. 2011. Comparison of the effects of environmental parameters on growth rates of *Vibrio vulnificus* biotypes I, II, and III by culture and quantitative PCR analysis. Appl Environ Microbiol 77:4200–4207.

682 23. Ramirez GD, Buck GW, Smith AK, Gordon KV, Mott JB. 2009. Incidence of *Vibrio*
683 *vulnificus* in estuarine waters of the south Texas Coastal Bend region. J Appl
684 Microbiol 107:2047–2053.

685 24. Johnson CN, Flowers AR, Noriea NF, Zimmerman AM, Bowers JC, DePaola A,
686 Grimes DJ. 2010. Relationships between environmental factors and pathogenic
687 vibrios in the northern Gulf of Mexico. Appl Environ Microbiol 76:7076–7084.

688 25. Nigro OD, Hou A, Vithanage G, Fujioka RS, Steward GF. 2011. Temporal and
689 spatial variability in culturable pathogenic *Vibrio* spp. in Lake Pontchartrain,
690 Louisiana, following hurricanes Katrina and Rita. Appl Environ Microbiol
691 77:5384–5393.

692 26. Wetz JJ, Blackwood AD, Fries JS, Williams ZF, Noble RT. 2014. Quantification of
693 *Vibrio vulnificus* in an estuarine environment: a multi-year analysis using qPCR.
694 Estuaries Coasts 37:421–435.

695 27. Dziuban EJ, Liang JL, Craun GF, Hill V, Yu PA, Painter J, Moore MR, Calderon RL,
696 Roy SL, Beach MJ, Control C for D, CDC P. 2006. Surveillance for waterborne
697 disease and outbreaks associated with recreational water—United States,
698 2003–2004. MMWR Surveill Summ Morb Mortal Wkly Rep Surveill Summ CDC
699 55:1–30.

700 28. Yoder JS, Hlavsa MC, Craun GF, Hill V, Roberts V, Yu PA, Hicks LA, Alexander NT,
701 Calderon RL, Roy SL, Beach MJ, Control C for D, CDC P. 2008. Surveillance for
702 waterborne disease and outbreaks associated with recreational water use and
703 other aquatic facility-associated health events—United States, 2005–2006.
704 MMWR Surveill Summ Morb Mortal Wkly Rep Surveill Summ CDC 57:1–29.

705 29. Hlavsa MC, Roberts VA, Anderson AR, Hill VR, Kahler AM, Orr M, Garrison LE,
706 Hicks LA, Newton A, Hilborn ED, Wade TJ, Beach MJ, Yoder JS, CDC. 2011.
707 Surveillance for waterborne disease outbreaks and other health events

associated with recreational water—United States, 2007–2008. MMWR Surveill Summ Morb Mortal Wkly Rep Surveill Summ CDC 60:1–32.

30. Vithanage G. 2011. The prevalence and public health significance of human pathogenic *Vibrio* species (*V. cholera*, *V.vulnificus*, *V. parahaemolyticus*, *V. alginolyticus*) in Hawai'i's diverse tropical coastal environments. PhD Thesis, University of Hawai'i at Mānoa, Honolulu.

31. Viau EJ, Goodwin KD, Yamahara KM, Layton BA, Sassoubre LM, Burns SL, Tong H-I, Wong SHC, Lu Y, Boehm AB. 2011. Bacterial pathogens in Hawaiian coastal streams–associations with fecal indicators, land cover, and water quality. Water Res 45:3279–3290.

32. Giambelluca TW, Chen Q, Frazier AG, Price JP, Chen YL, Chu PS, Eischeid JK, Delparte DM. 2013. Online rainfall atlas of Hawai'i. Bull Am Meteorol Soc 94:313–316.

33. De Carlo EH, Anthony SS. 2002. Spatial and temporal variability of trace element concentrations in an urban subtropical watershed, Honolulu, Hawaii. Appl Geochem 17:475–492.

34. De Carlo EH, Anthony SS. 2002. Spatial and temporal variability of trace element concentrations in an urban subtropical watershed, Honolulu, Hawaii. Appl Geochem 17:475–492.

35. Laws EA, Doliente D, Hiayama J, Hokama M-L, Kim K, Li D, Minami S, Morales C. 1993. Hypereutrophication of the Ala Wai Canal, Oahu, Hawaii: prospects for cleanup. Pac Sci 47:59–75.

36. Gonzales F. 1971. A descriptive study of the physical oceanography of the Ala Wai Canal. PhD Thesis, University of Hawa'i at Mānoa, Honolulu.

37. Gordon LI, Jennings Jr JC, Ross AA, Krest JM. 1994. A suggested protocol for

733 continuous flow automated analysis of seawater nutrients (phosphate, nitrate,
734 nitrite and silicic acid) in the WOCE Hydrographic Program and the Joint Global
735 Ocean Flux Study. 93–1. Technical Report, Oregon State University, College of
736 Oceanography, Descriptive Chemical Oceanography Group.

737 38. Tomlinson MJ, De Carlo EH, McManus MA, Pawlak G, Steward GF, Sansone FJ,
738 Nigro OD, Timmerman RE, Patterson J, Jaramillo S, Ostrander CE. 2011.
739 Characterizing the effects of two storms on the coastal waters of O'ahu, Hawai'i,
740 using data from the Pacific Islands Ocean Observing System. Oceanography
741 24:182–199.

742 39. Karl DM, Dore JE, Hebel DV, Winn C. 1991. Procedures for particulate carbon,
743 nitrogen, phosphorus and total mass analyses used in the US-JGOFS Hawaii
744 Ocean Time-series program, p. 71–77. *In* Hurd, DC, Spencer, DW (eds.), Marine
745 Particles: Analysis and Characterization. Washington, D.C.

746 40. Strickland JDH, Parsons TR. 1972. A practical hand book of seawater analysis,
747 2nd ed. Fisheries Research Board of Canada Bulletin 157.

748 41. Berthelet M, Whyte LG, Greer CW. 1996. Rapid, direct extraction of DNA from
749 soils for PCR analysis using polyvinylpolypyrrolidone spin columns. FEMS
750 Microbiol Lett 138:17–22.

751 42. Campbell MS, Wright AC. 2003. Real-time PCR analysis of *Vibrio vulnificus* from
752 oysters. Appl Environ Microbiol 69:7137–7144.

753 43. Baker-Austin C, Gore A, Oliver JD, Rangdale R, McArthur JV, Lees DN. 2010.
754 Rapid in situ detection of virulent *Vibrio vulnificus* strains in raw oyster
755 matrices using real-time PCR. Environ Microbiol Rep 2:76–80.

756 44. Bustin SA, Benes V, Garson JA, Hellemans J, Huggett J, Kubista M, Mueller R,
757 Nolan T, Pfaffl MW, Shipley GL, Vandesompele J, Wittwer CT. 2009. The MIQE
758 Guidelines: Minimum information for publication of quantitative real-time PCR

759 experiments. Clin Chem 55:611–622.

760 45. Deeb R, Tufford D, Scott GI, Moore JG, Dow K. 2018. Impact of climate change on
761 *Vibrio vulnificus* abundance and exposure risk 1–15.

762 46. Banakar V, Constantin de Magny G, Jacobs J, Murtugudde R, Huq A, Wood RJ,
763 Colwell RR. 2011. Temporal and spatial variability in the distribution of *Vibrio*
764 *vulnificus* in the Chesapeake Bay: a hindcast study. EcoHealth 8:456–467.

765 47. Parvathi A, Kumar HS, Karunasagar I, Karunasagar I. 2004. Detection and
766 enumeration of *Vibrio vulnificus* in oysters from two estuaries along the
767 southwest coast of India, using molecular methods. Appl Environ Microbiol
768 70:6909–6913.

769 48. De Carlo EH, Hoover DJ, Young CW, Hoover RS, Mackenzie FT. 2007. Impact of
770 storm runoff from tropical watersheds on coastal water quality and
771 productivity. Appl Geochem 22:1777–1797.

772 49. Goldberg S, Sposito G. 1984. Chemical model of phosphate adsorption by soils:
773 I. Reference oxide minerals. Soil Sci Soc Am J 48:772–778.

774 50. Creamer B. 2006. Bacteria draw attention of UH scientists. Honol Advert.
775 Honolulu.

776 51. Williams TC, Froelich BA, Phippen B, Fowler P, Noble RT, Oliver JD. 2017.
777 Different abundance and correlational patterns exist between total and
778 presumed pathogenic *Vibrio vulnificus* and *V. parahaemolyticus* in shellfish and
779 waters along the North Carolina coast. FEMS Microbiol Ecol 93:125–11.

780 52. Lin M, Schwarz JR. 2003. Seasonal shifts in population structure of *Vibrio*
781 *vulnificus* in an estuarine environment as revealed by partial 16S ribosomal
782 DNA sequencing. FEMS Microbiol Ecol 45:23–27.

783 53. Maugeri TL, Carbone M, Fera MT, Gugliandolo C. 2006. Detection and
784 differentiation of *Vibrio vulnificus* in seawater and plankton of a coastal zone of
785 the Mediterranean Sea. Res Microbiol 157:194–200.

786 54. Jacobs JM, Rhodes M, Brown CW, Hood RR, Leight A, Long W, Wood R. 2014.
787 Modeling and forecasting the distribution of *Vibrio vulnificus* in Chesapeake
788 Bay. J Appl Microbiol 117:1312–1327.

789

790 **Table 1.** Variables measured on individual samples, the number of samples measured, and the
791 geometric mean (geomean), mean, median, minimum (min) and maximum (max) values for each
792 (reported to two significant digits).

| Variable | units | n | Geomean | Mean | Median | S.D. | Min | Max |
|---|---|---|---|---|---|---|---|---|
| Temperature | °C | 242 | 27 | 27 | 27 | 2.6 | 19 | 32 |
| Salinity | ppt | 243 | 20 | 24 | 28 | 9.7 | 1 | 36 |
| Nitrate | µM | 209 | 18 | 37 | 17 | 48 | 0.02 | 260 |
| Nitrite | µM | 211 | 0.47 | 0.59 | 0.47 | 0.47 | 0.04 | 3.3 |
| Ammonia | µM | 207 | 5.5 | 6.7 | 5.7 | 4.3 | 0.94 | 22 |
| Phosphate | µM | 211 | 1 | 1.3 | 0.95 | 1.1 | 0.2 | 8.7 |
| Silica | µM | 211 | 110 | 140 | 120 | 92 | 11 | 490 |
| Particulate Carbon | µM | 199 | 130 | 250 | 120 | 650 | 20 | 7500 |
| Particulate Nitrogen | µM | 199 | 16 | 26 | 14 | 51 | 2.6 | 560 |
| Chlorophyll *a* | $\mu g\ L^{-1}$ | 194 | 7.6 | 19 | 7.3 | 43 | 0.4 | 500 |
| Total bacteria | $10^9$ cells $L^{-1}$ | 219 | 4.2 | 4.8 | 4.7 | 2.3 | 0.47 | 11 |
| CaV blue[1] | CFU $mL^{-1}$ | 59 | 130 | 400 | 100 | 770 | 12 | 3904 |
| *vvhA* gene[2] | copies $mL^{-1}$ | 239 | 68 | 330 | 60 | 1200 | 3.4 | 14000 |

793 [1] culture-based blue colony forming units (CFU) when plating on CHROMagar Vibrio medium (CaV)
794 [2] qPCR-based estimates
795

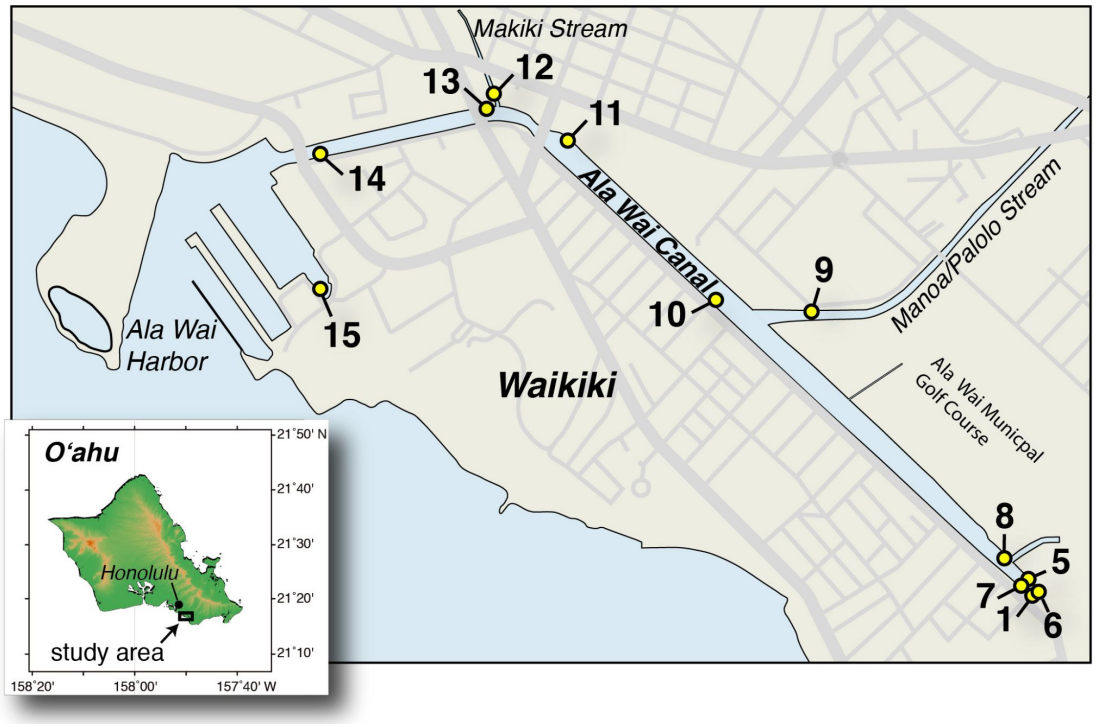


796

797 **Fig. 1.** Map of Samping Sites. Inset shows the general location of the canal on the
798 south shore of the island of O'ahu in the Hawaiian Island chain. Main map shows the
799 site numbers and position along the canal. Site 1 is at the closed end of the canal
800 with occasional input from surface runoff via storm drains. Sites 9 and 12 are at the
801 mouths of the Mānoa-Pālolo and Makiki Streams, respectively.

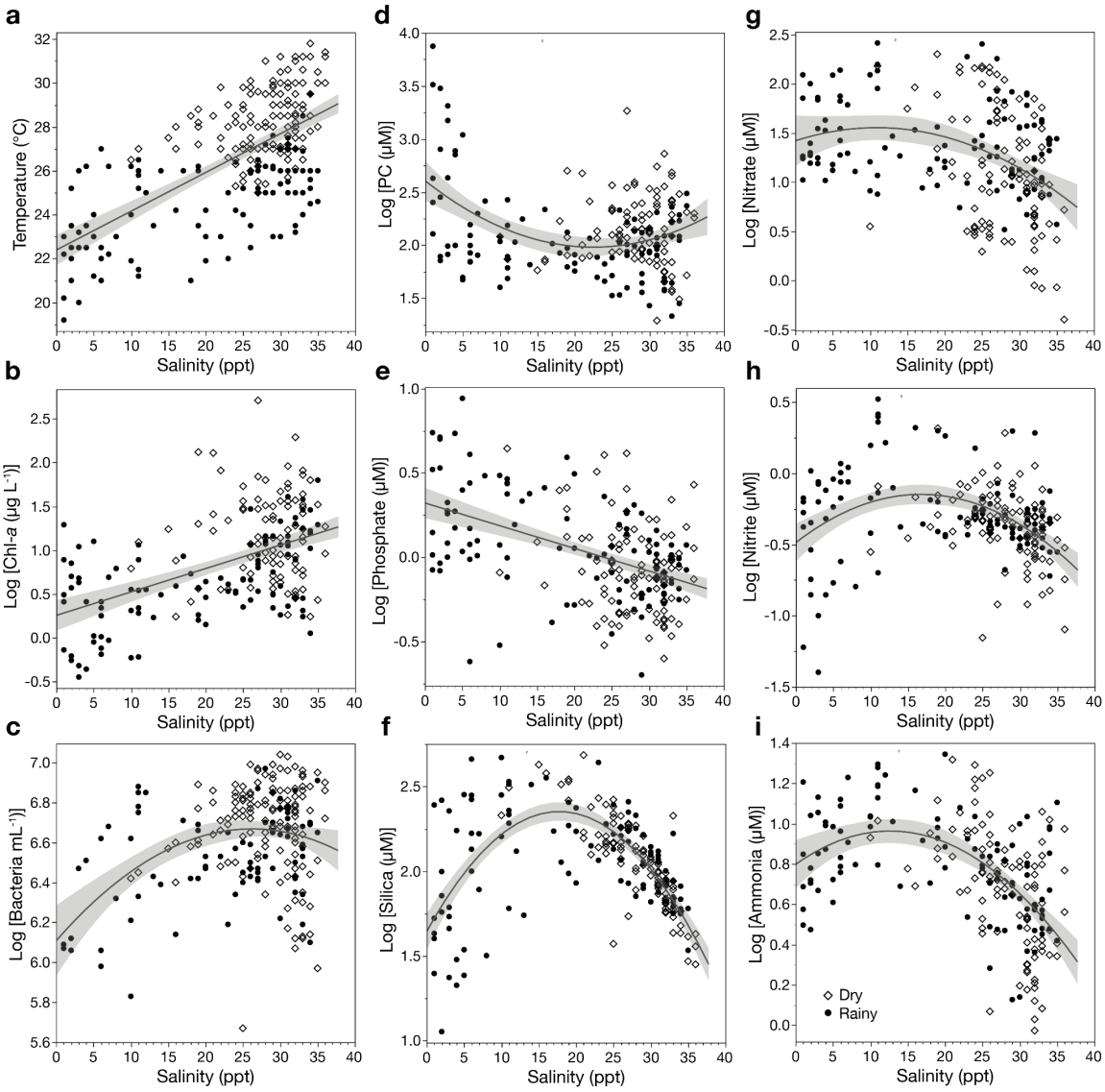


**Fig. 2.** Variability in measured biological and chemical properties of samples as a function of salinity in samples from the rainy (solid circles) and dry (open diamonds) seasons. Regressions against salinity are shown for (**a**) temperature ($r^2$ = 0.42), (**b**) Log chl *a* ($r^2$ = 0.24), (**c**) log bacteria ($r^2$ = 0.14), (**d**) log PC ($r^2$ = 0.13), (**e**) log phosphate ($r^2$ = 0.22), (**f**) log silica ($r^2$ = 0.463), (**g**) log nitrate ($r^2$ = 0.13), (**h**) log nitrite ($r^2$ = 0.152), (**i**) log ammonia ($r^2$ = 0.29). Regression lines and 95% confidence limits were fit using only first order terms unless addition of a quadratic term substantially improved $r^2$ or reduced root mean square error. All fits were significant ($p < .0001$).

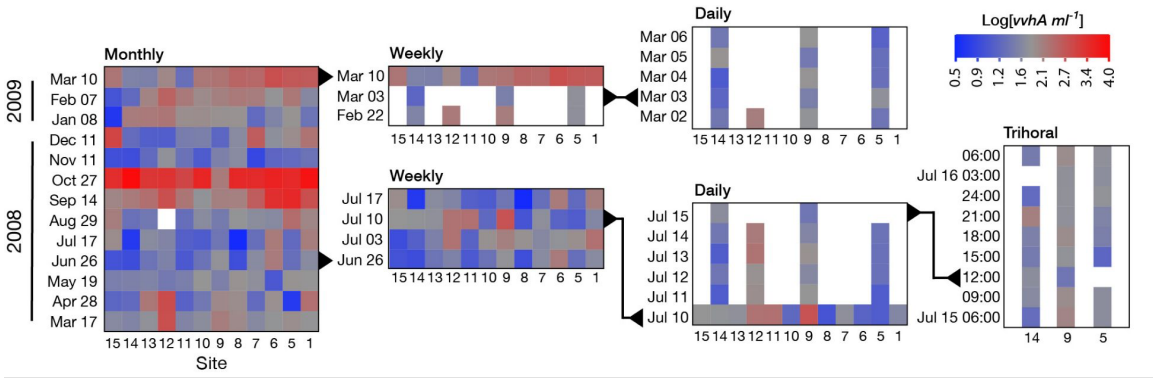


**Fig. 3.** Heat maps illustrating spatial and temporal variability in *V. vulnificus*. Log *vvhA* concentrations are color coded at each station over time for monthly, weekly, daily and trihoral sampling events. The overall average log(*vvha*) from all samplings of 1.8 is shown in grey. Concentrations above average are in red and those below average in blue. The samplings on different time scales are nested and the events that are overlapping in the different graphs are indicated with black triangles and lines.

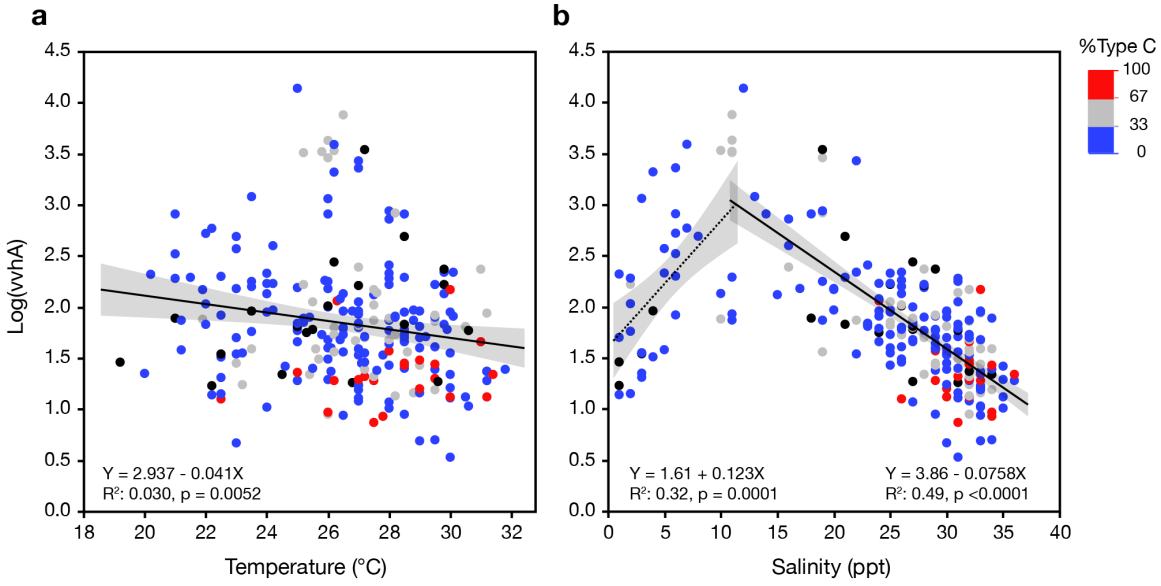


**Fig. 4.** Concentration of *vvhA* as a function of **a**) temperature or **b**) salinity. The percentage of total *vvhA* that derives from "C-type" *V. vulnificus* was determined as the ratio of *vcgC* (C-type) and *vvhA* (total V. vulnificus) gene concentrations and is indicated by the color scale. Blue dots are samples dominated by E-type, red dots by C-type. Black dots are samples for which the % C-type could not be determined because of missing data.

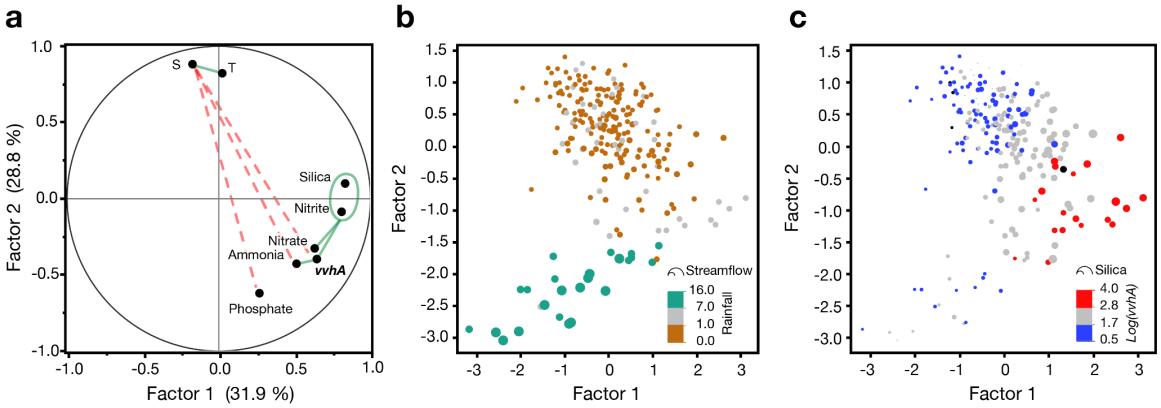


**Fig. 5.** Factor Analysis for *vvhA*, temperature, salinity, and nutrients. (**a**) The factor loading plot for factors 1 and 2 (eigenvalues >1). Variables with a strong positive correlations (r ≥ 0.4) are connected by green solid lines and those with strong negative correlation (r ≤ 0.4) are connected by dashed red lines (**b**) Plot of the factor scores for the data with points colored by 24-hr antecedent rainfall in Mānoa Valley (in cm) and scaled in size so area is proporional to streamflow in the Mānoa-Pālolo Stream. (**c**) Plot of the factor scores with data points colored according to log *vvhA* concentration and scaled in size so area is proportional to silica concentration.

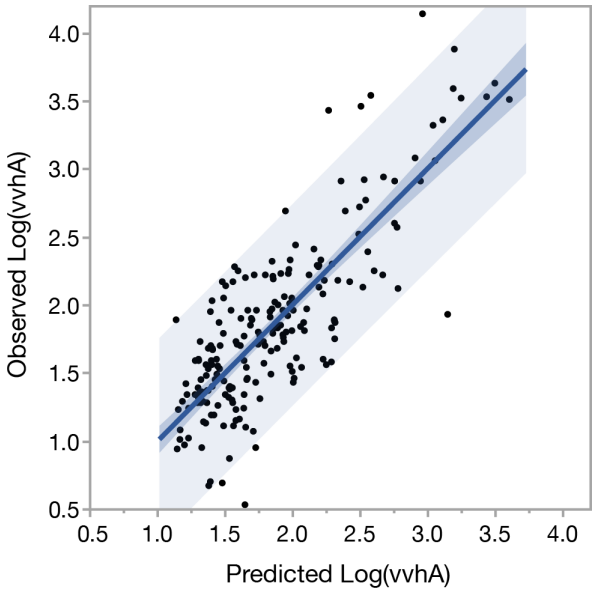


835

836 **Fig. 6.** Observed vs. predicted values of log transformed *vvhA* gene copies per $mL^{-1}$.
837 Predicted values are combined from two separate models (one for samples < 12 ppt, one for
838 ≥ 12 ppt). Predicted values are restricted to individual samples for which all of the predictor
839 variables were measured within a given salinity range (n = 204 out of 239 in total). Darker
840 and lighter shading illustrates the 95% confidence limits of the fit and prediction,
841 respectively. Combined, the models explain a significant amount of the variation in the
842 observations: $r^2 = 0.661$, RMSE = 0.37, F Test (1, 204) = 396.90, $p < .0001$.

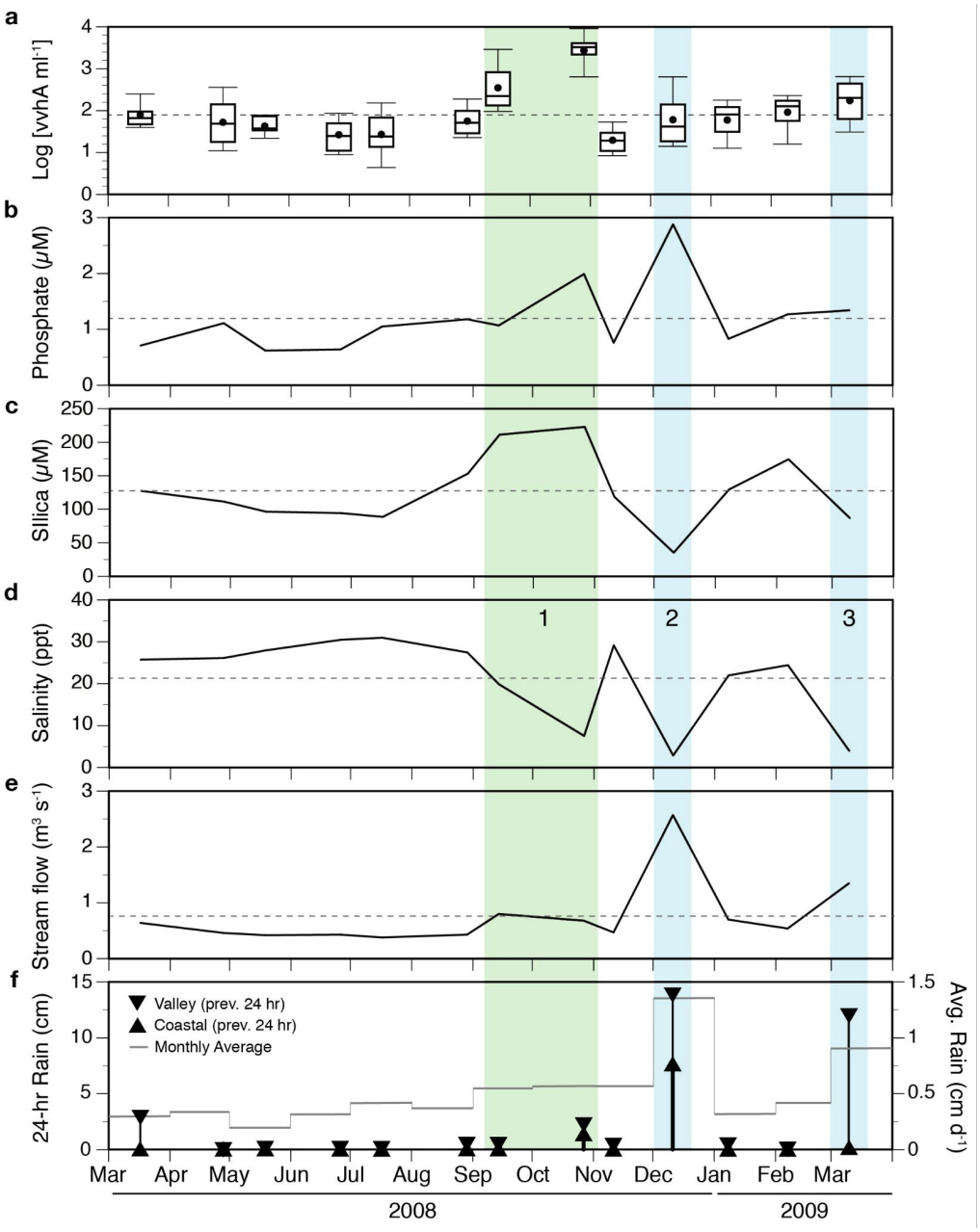


843

844 **Fig. 7.** Time series of variables in or influencing the Ala Wai Canal system. Shown are **a**)
845 variations of *vvhA* concentrations as box plots of all log transformed values measured at
846 every site at each monthly sampling, canal-wide geometric means of **b**) phosphate, **c**)
847 salinity, **d**) silica, as well as **e**) streamflow in the Mānoa-Pālolo stream on the day of
848 sampling, and **f**) rainfall in the 24-hr period preceding sampling as measured at the
849 Honolulu coastal (upward triangles) and Mānoa Valley rain gauges (downward triangles).
850 Daily rainfall average for the month is shown as the mean for both sites (grey line). Dashed
851 lines in **a-e** show the mean value over the time period.

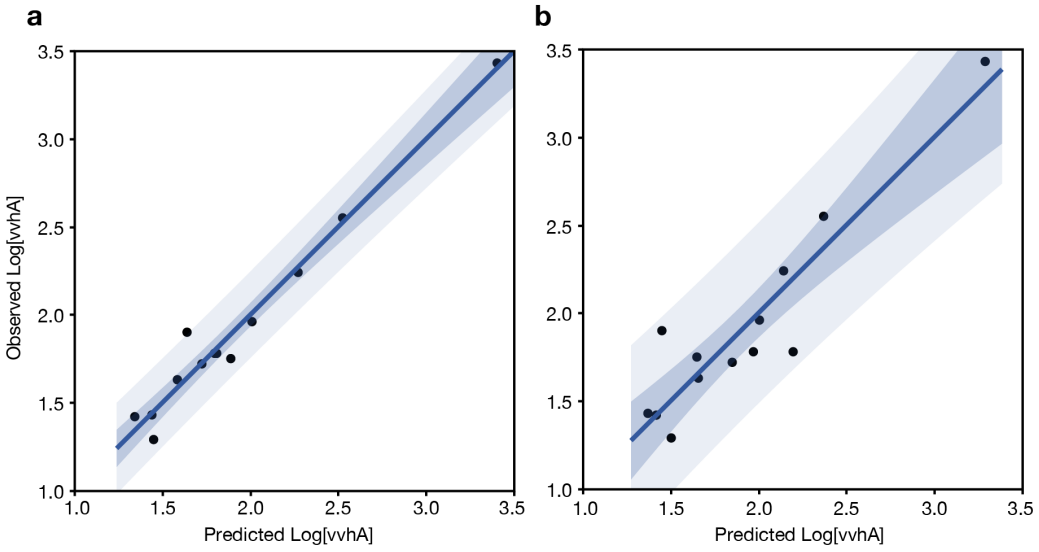


852

853 **Fig. 8.** Observed vs predicted canal-wide average of log-transformed *vvhA* concentrations.
854 Predictions are derived from **a**) the best subset of variables (salinity, silica, streamflow,
855 particulate carbon) from generalized regression model ($r^2$ = 0.97; RMSE = 0.11; F test p <
856 .0001) or **b**) a restricted subset of two variables (rainfall and salinity) that are easily
857 measured autonomously ($r^2$ = 0.86; RMSE = 0.22; F test p <.0001). Darker and lighter
858 shading illustrates the 95% confidence limits of the fit and prediction, respectively.